Smart Structures and Systems, *Vol. 24, No. 6 (2019) 693-707*
DOI: https://doi.org/10.12989/sss.2019.24.6.693

Multi-sensor data fusion based assessment on shield tunnel safety

Hongwei Huang[1a], Xin Xie[1b], Dongming Zhang[*1], Zhongqiang Liu[2c] and Suzanne Lacasse[2d]

[1]*Department of Geotechnical Engineering, Tongji University, 1239 Siping Rd, Shanghai 200092, China*
[2]*Natural Hazards, Norwegian Geotechnical Institute (NGI), 3930 Ullevaal St., NO-0806 Oslo, Norway*

(Received July 3, 2019, Revised August 9, 2019, Accepted August 29, 2019)

Abstract. This paper proposes an integrated safety assessment method that can take multiple sources data into consideration based on a data fusion approach. Data cleaning using the Kalman filter method (KF) was conducted first for monitoring data from each sensor. The inclination data from the four tilt sensors of the same monitoring section have been associated to synchronize in time. Secondly, the finite element method (FEM) model was established to physically correlate the external forces with various structural responses of the shield tunnel, including the measured inclination. Response surface method (RSM) was adopted to express the relationship between external forces and the structural responses. Then, the external forces were updated based on the in situ monitoring data from tilt sensors using the extended Kalman filter method (EKF). Finally, mechanics parameters of the tunnel lining were estimated based on the updated data to make an integrated safety assessment. An application example of the proposed method was presented for an urban tunnel during a nearby deep excavation with multiple source monitoring plans. The change of tunnel convergence, bolt stress and segment internal forces can also be calculated based on the real time deformation monitoring of the shield tunnel. The proposed method was verified by predicting the data using the other three sensors in the same section. The correlation among different monitoring data has been discussed before the conclusion was drawn.

Keywords: shield tunnel; data fusion; extended Kalman filter; safety assessment

1. Introduction

As the mainstay of urban transportation, metro tunnels are often designed for service periods of over 100 years. During the operational period, the urban tunnels undergo long term loads, material aging, environmental corrosion and even extreme loads. Increasing attention has been drawn on the maintenance of metro tunnel as any accidents would cause unacceptable casualties and economic losses (Frangopol 2008).

Segment tunnel structures are sensitive to the ambient stress caused by nearby construction such as foundation pit excavation, surcharging and tunneling (Lin *et al.* 2007, Huang *et al.* 2017, Zhang *et al*. 2013). With the rapid development of sensing technology, structure health monitoring (SHM) has become a central technology to mitigate potential hazards (Bhalla *et al.* 2005, Bennett *et al.* 2010a, Bennett *et al.* 2010b, Ye *et al*. 2013, Wang *et al.* 2016, Ye *et al*. 2016). The SHM system also provides sufficient data resources to study the long-term tunnel performance and even a potential disaster evolution. Therefore, the SHM technology has attracted increasing research interests in researcher worldwide, and has been widely used for application in the past few decades. The objective of SHM is to detect the structural damage and degradation with the help of in-situ, nondestructive sensing and mechanical analysis (Housner *et al*. 1997). The measured data are often used as an reference index for safety assessment, damage detection, decision making, model updating and health diagnosis (Yang *et al*. 2005, Mair *et al.* 2008, Mohamad *et al.* 2012, Hu *et al.* 2013, Torbol *et al.* 2013, Santos *et al*. 2012, Ye *et al*. 2015). There are usually four parts in an SHM system: sensors, hardware and software of data acquisition, transmission and processing units, and data management systems (Ou 2003). Multi-source sensing technology has often been used in a SHM system to improve the reliability and accuracy. Although sensors were installed for different measuring purposes, they reflect different characteristics of the geotechnical structures. Many researchers pointed out that an integral safety assessment using multiple sources of monitoring information may be more reasonable and reliable than single index assessment (Peng *et al.* 2014, Li *et al.* 2016a), because it will also provide a more comprehensive understanding of the tunnel mechanical performance and the evolution process of a potential disaster.

Multi-sensor fusion technique integrates data from multiple sensors in a monitoring system and other related information to achieve improved accuracy and more specific inferences that cannot be achieved with single sensor alone (Walz and Llinas 1990, Hall and Llinas 1998). In the past decade, the multi-sensor fusion method has often been used to improve the performance of the monitoring

*Corresponding author, Assistant Professor
E-mail: 09zhang@tongji.edu.cn
[a] Professor
[b] Ph.D. Student
[c] Senior Adviser
[d] Expert Adviser

ISSN: 1738-1584 (Print), 1738-1991 (Online)

system. Sun *et al.* (2012) proposed a data fusion method to improve the recognition accuracy of a pipeline monitoring system. Erazo and Hernandez (2016) proposed a data fusion based framework to estimate seismic induced damage in buildings. Santos *et al.* (2012) combined the data fusion method with pattern recognition and established a reliable method for early damage detection of a cable stayed bridge. The data fusion method can be used for safety assessment during the construction or operational period of a geotechnical structure. Chen *et al.* (2017) used the support vector machines approach (SVM) to identify anomalies monitoring data of deep excavation. To quantify the parameter uncertainties and make a full safety assessment of slope, Peng *et al.* (2014) and Li *et al.* (2016b) conducted a Bayesian networks model to fuse monitoring information from different sensors of a slope. Research on data fusion process has, however, been seldom conducted for a tunnel during operational period.

In this study, a systematic approach utilizing multi-source monitoring information with Kalman filter is proposed for the evaluation of shield driven tunnel safety. The method aims to (1) integrate multi-source information on tunnel loading characteristics; (2) update key external force changes such as the coefficients of lateral earth pressure; (3) analyze, from a perspective of inverse problem, the external forces imposed by construction nearby. An example of a shield tunnel with multiple monitoring derived indices is presented to illustrate the proposed methodology.

2. Methodology

2.1 The framework

A general framework of the proposed multi-sensor fusion method is shown in Fig. 1. In situ data are collected using different sensors within a real time monitoring system in a shield tunnel. There are three steps in the multi-sensor fusion process. (1) data preprocessing. It contains two parts: data cleaning and data association. Data cleaning is conducted to reduce the influence of data fluctuation caused by train vibration. The time-dependent data are associated to ensure consistency in time. (2) numerical simulation. Numerical model using the Finite Element Method (FEM) is established based on the real tunnel structure and the nearby construction condition. The relationships between the external force changes and the structural responses of the tunnel are studied using the numerical model and fitted using the polynomial function. (3) multi-sensor fusion. Extended Kalman filter (EKF) method is used to merge the different monitoring data and update the external forces of the tunnel. Other structural responses such as tunnel convergence, internal forces and joint opening are updated using the EKF. After that, a holistic safety assessment can be conducted based on these mechanical parameters.

In this paper, four mechanical indicators have been taken into consideration namely: tunnel convergence, joint opening, segmental internal forces and bolt stress as shown in Fig.1. Among these indicators, tunnel convergence and

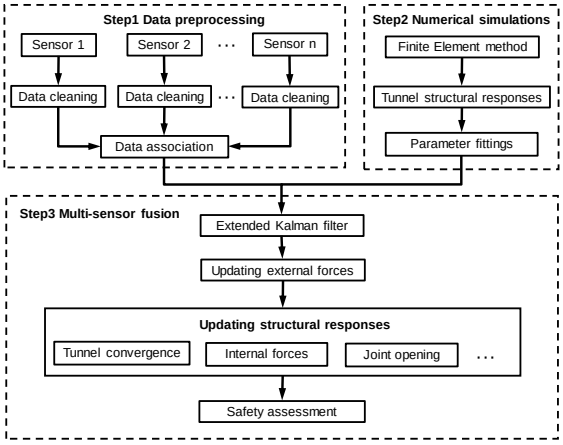

Fig. 1 Framework of the proposed method

joint opening are often seen as Key Performance Indicator (KPI) both for serviceability and safety limits. Different levels of the magnitude for the indicators can be adopted depending on the specific condition of application. British Tunnel Standards (BTS. 2004) sets an ultimate limit of convergence at 2% of the initial outer convergence, while Chinese code (GB50157. 2013) sets 0.5% of the convergence as the serviceability limits. The ultimate intrusive water pressure has a relationship with the joint opening width. The limit state of joint opening is determine based on the ultimate intrusive water pressure and the in-situ water pressure. Bolt stress and internal forces which are difficult to measure in the tunnel structure can also be calculated using the proposed method.

Although the Kalman filter approach has been used for step 1 and step 3, the function of Kalman filter are different. Kalman filter is adopted for data cleaning in the first step whereas the method is used to merge different monitoring data in step 3. More detail information about proposed method will be introduced in the following subsections.

2.2 Data preprocessing

The raw data of each sensor should be cleaned and associated in time before the data fusion process is undertaken. The Kalman filter is one of the most widely used techniques to do data cleaning (Kalman 1960).

In the Kalman filter process, the predicted data at time k+1 is equal to the recent state

$$\hat{x}(k+1|k) = \hat{x}(k|k) \tag{1}$$

where $\hat{x}(k+1|k)$ is the predicted monitoring data at time k+1 using the in situ monitoring data at time k, and $\hat{x}(k+1|k)$ means the estimated data at time k+1 using the data of time k.

The predicted covariance of x is expressed as

$$P(k+1|k) = P(k|k) + Q \tag{2}$$

where $P(k+1|k)$ is the predicted covariance at time k+1 and $P(k|k)$ is the estimated covariance at time k.

Then Kalman gain K is calculated using the predicted covariance

$$K = P(k+1|k)H^T\left[HP(k+1|k)H^T + R\right]^{-1} \quad (3)$$

where R is the covariance of the observation error, $P(k+1|k)$ is the predicted covariance and H is a unit matrix.

The state of parameter x can be updated using the Kalman gain

$$\hat{x}(k+1|k+1) = \hat{x}(k+1|k) + K\left[x(k+1) - \hat{x}(k+1|k)\right] \quad (4)$$

The covariance of x can be updated using the following formula

$$P(k+1) = \left[I - K*H\right]P(k+1|k) \quad (5)$$

By iterating calculations 1 to 5, the data are filtered by alternating prediction and calibration. With the iterations, the curve with the data in the real time becomes more smooth as the Kalman filter is repeatedly applied.

Although different sensors in the same section has the same monitoring frequency, the data from different sensors are not always synchronized in time. In practical application, some of the data are even incomplete due to monitoring and data transmission reasons. To compensate for this, data association should be conducted to synchronize the data in time. Either nonlinear or linear interpolation methods can be adopted depending on the condition of data trend. For the stable trend of data, linear interpolation is a good choice for its simplicity, while nonlinear interpolation should be adopted when data exhibits higher complexity and nonlinear variation trend. Considering of the page limit, it is not explained further in this paper.

2.3 Numerical simulation and parameter fitting

Nearby construction may cause a distinct change in tunnel external forces and lead to a response in tunnel deformation. Numerical simulation using the finite element method is conducted under the loading condition of the tunnel. For example, as illustrated in Fig. 2, a simplified model is established to simulate a urban tunnel with nearby pit excavation. The coefficient of lateral soil pressure K_0 of both sides are chosen as the key external forces for the case of a foundation pit excavation near the tunnel (Doležalov *et al.* 2001). The coefficient of lateral soil pressure is defined as the ratio of the effective horizontal to vertical stress, $K_0=\sigma'_h/\sigma'_v$. Please note that the external forces should not necessarily be the K_0 for other problems.

The relationship between the external forces and the tunnel mechanical indices such as segment rotation, tunnel convergence, joint opening and bolt stress are calculated with the result of numerical simulation. Data fitting techniques such as the response surface function method and polynomial fitting can be used to reflect these

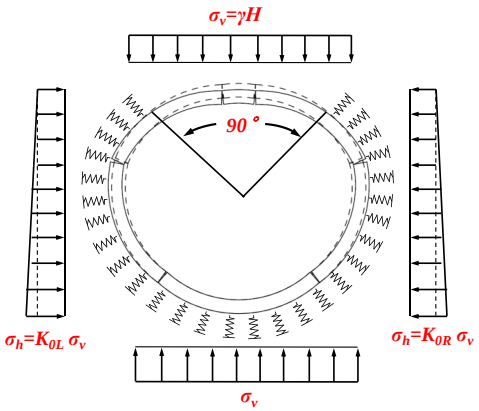

Fig. 2 Load-structure model for shield tunnel and the K0 on left and right sides

relationships (Bucher and Bourgund 1990, Bucher and Most 2008). Hence structural responses can be calculated by tunnel external forces using polynomials as

$$g(\boldsymbol{x}) = \sum_{i=1}^{m}\alpha_{ni}x_i^{\,n} + \sum_{i=1}^{m}\alpha_{(n-1)i}x_i^{\,n-1} + \mathrm{L} + \sum_{i=1}^{m}\alpha_{1i}x_i + \alpha_0 \quad (6)$$

where $\boldsymbol{x}$=(x_1, x_2,…x_m) are the external forces, in example $x_1=K_{0L}$ $x_2=K_{0R}$ for the case of a foundation pit excavation near the tunnel.

It should be noted that the observations from multi sensors $\boldsymbol{y}$ are included in the structural responses. So the monitoring data can also be calculated using the polynomial functions

$$\boldsymbol{y} = \boldsymbol{g}(\boldsymbol{x}) = \boldsymbol{g}(x_1, x_2 \mathrm{L}\ x_m) \quad (7)$$

2.4 Updating external forces and calculating performance index

The Kalman filter method is applicable for a linear system. This is not applicable for the polynomial relationship of the parameters. The extended Kalman filter method (*EKF*) is then used to solve the polynomial equation (Wang *et al.* 2014). The observation data can be expressed with the fitting functions in Eq. (7) and the observational error (Welch and Bishop 2001)

$$\boldsymbol{y}(k) = \boldsymbol{g}(\boldsymbol{x}(k)) + \boldsymbol{v}_t \quad (8)$$

where $\boldsymbol{y}(k)$ is the monitoring vector from multi sensors at time k, $\boldsymbol{x}(k)$ is the unknown external forces at time k, $\boldsymbol{g}(x)$ is the fitting functions using RSM or other polynomial function, $\boldsymbol{v}_t$ is the observational error vector.

And the external force vectors $\boldsymbol{x}$ at time k+1 can be estimated using the $\boldsymbol{x}$ from the previous time

$$\boldsymbol{x}(k+1) = \boldsymbol{x}(k) + \boldsymbol{w}_t \quad (9)$$

where $\boldsymbol{w}_t$ is systematic error which is often assumed to follow an unbiased normal distribution.

The main steps of the extended Kalman filter method is similar to the Kalman filter method as shown in Eqs. (1) to (5) However, the estimated value for the monitoring value is the polynomial function of $\boldsymbol{x}$. And the elements in matrix $\boldsymbol{H}$ in the *EKF* are computed using a first order Taylor series expansion

$$\boldsymbol{H}=\frac{\partial \boldsymbol{g}}{\partial \boldsymbol{x}}=\begin{bmatrix} \frac{\partial g_1}{\partial x_1} & \mathrm{L} & \frac{\partial g_1}{\partial x_m} \\ \mathrm{M} & \mathrm{O} & \mathrm{M} \\ \frac{\partial g_n}{\partial x_1} & \mathrm{L} & \frac{\partial g_n}{\partial x_m} \end{bmatrix} \tag{10}$$

where $\boldsymbol{g}$ is the fitting functions in equation (7), $\boldsymbol{x}$ is the external force vectors at time k.

The Kalman gain is calculated using the matrix $\boldsymbol{H}$

$$\boldsymbol{K}=P(k+1|k)\boldsymbol{H}^T\left[\boldsymbol{H}P(k+1|k)\boldsymbol{H}^T+R\right]^{-1} \tag{11}$$

Then external forces of the tunnel are updated using the Kalman gain and the monitoring data

$$\hat{\boldsymbol{x}}(k+1|k+1)=\hat{\boldsymbol{x}}(k+1|k)+\boldsymbol{K}\left[\boldsymbol{y}(k+1)-\hat{\boldsymbol{y}}(k+1|k)\right] \tag{12}$$

where $\boldsymbol{y}(k+1)$ is the in situ monitoring data observed in time $k+1$.

The covariance of x in time k+1 is also updated using the approximate matrix $\boldsymbol{H}$ and the predicted covariance $P(k+1|k)$

$$P(k+1)=\left[I-\boldsymbol{K}*H\right]P(k+1|k) \tag{13}$$

Using the response surface function in Eq. (6), mechanical indices such as tunnel convergence, bolt stresses and joint opening can be updated. A safety assessment can be conducted using these performance indexes.

3. Application example

To illustrate the whole approach and applicability of the proposed data fusion based safety assessment, an example of data fusion of real time multi-sensor observations in a shield tunnel is now presented.

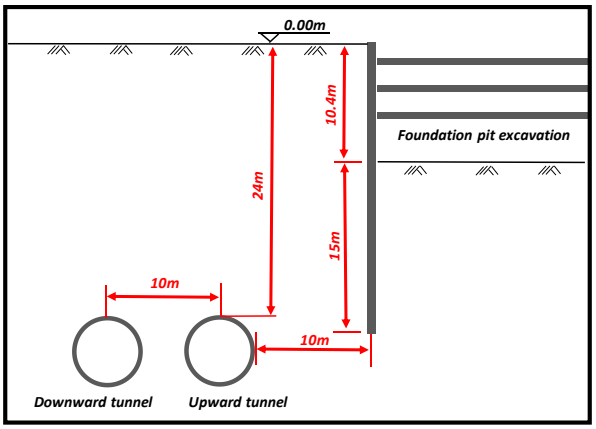

Fig. 3 Real time observations in four segments after synchronization of measurements in time

3.1 Project description

The monitoring was done in one of the tunnels of the Shanghai metro line 12. The tunnel was built by earth pressure balance shield machine in the end of 2012. The lining of the shield tunnel consists of six concrete segments which are prefabricated in the factory before tunneling. The tunnel is at an average depth of 20 m and has an outer diameter of 6.2 m. Nearby the tunnel as shown in Fig. 3, a large foundation pit, 100 m wide, 110 m long and at 20 depth, was under excavation between 9th January 2016 and 25th April 2016.

To mitigate the potential risk associated with the added stresses and to make a safety assessment of the tunnel during the excavation nearby, a real time monitoring system using wireless sensor network was installed to measure the deformation of the tunnel (Bennet *et al.* 2010, Huang *et al.* 2013, Wang *et al.* 2016). The ratio of convergence of the horizontal inner diameter is often taken as a key performance index (KPI) for the assessment of tunnel serviceability and safety (BTS. 2004; GB50157. 2013). Therefore, the horizontal convergence of the tunnel is often measured during the operational period (Mair 2008, Pinto and Whittle 2014, Huang *et al.* 2017). A novel monitoring method using wireless multi sensor system was developed to measure the rotation of the tunnel segments in real time. A geometric transformation was used to transform the rotation into tunnel horizontal convergence (Huang *et al.* 2013, Wang *et al.* 2016).

Fig. 4 shows that tilt sensors were installed at the L1, L2, B1 and B2 segments of Ring 805 in the monitored tunnel interval.

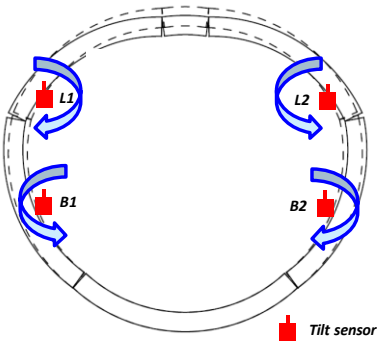

(a) Sensors layout sketch

(b) Actual tilt sensors

Fig. 4 Installing position of the tilt sensors

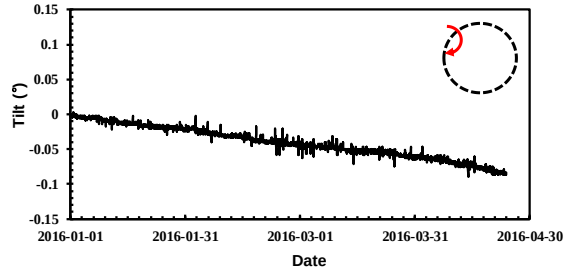

(a) Segment L1

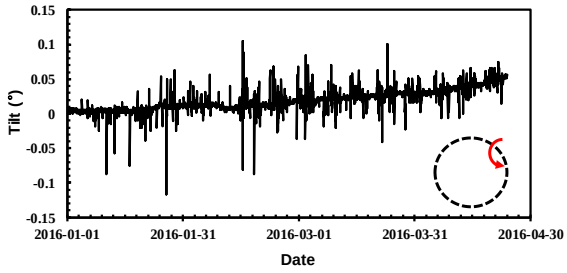

(b) Segment L2 (close to the excavating pit)

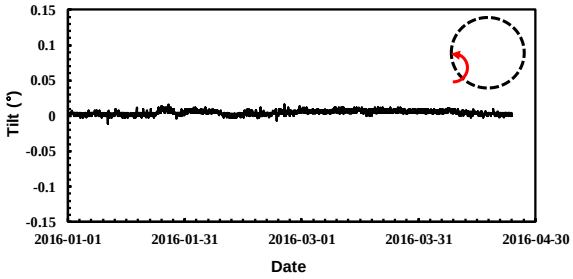

(c) Segment B1

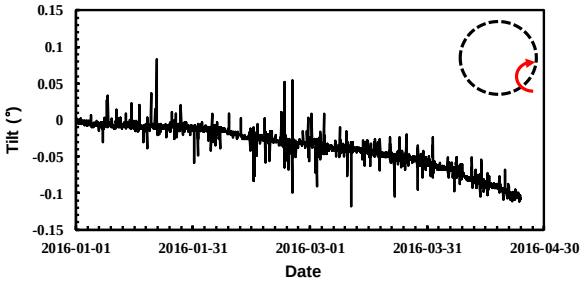

(d) Segment B2 (close to the excavating pit)

Fig. 5 Raw data of the tilt sensors at four segments during excavation period

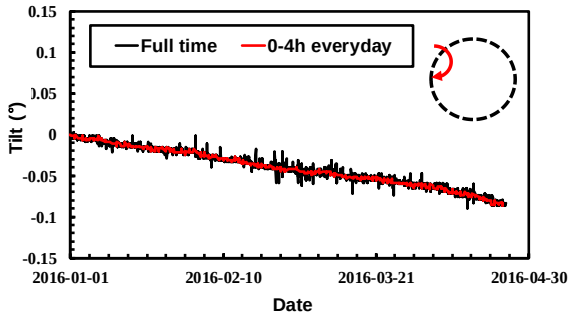

(a) Segment L1

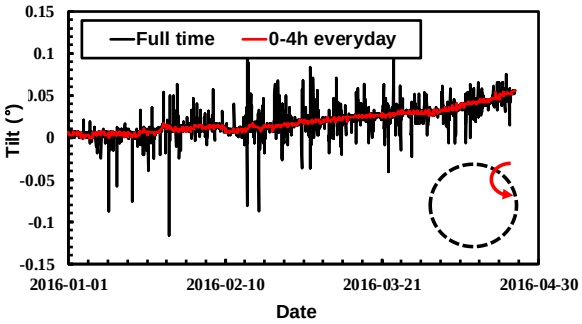

(b) Segment L2 (close to the excavating pit)

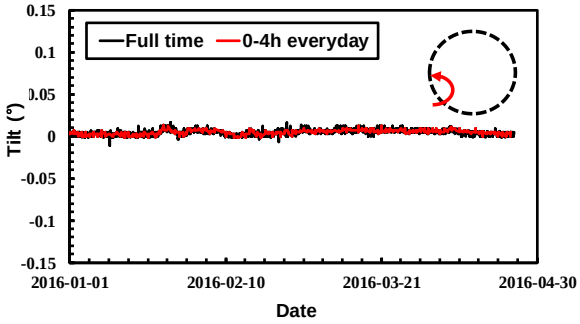

(c) Segment B1

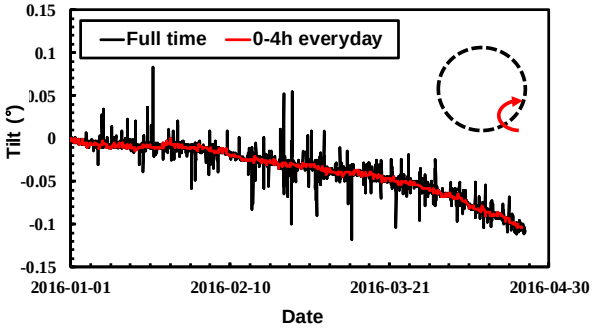

(d) Segment B2 (close to the excavating pit)

Fig. 6 Comparison of raw tilt data during the non-operational and operational period

The excavation was undertaken on the right side of the tunnel in Fig. 4. Tilt data were collected every one hour between 1st January and 25th April 2016. For each tilt sensors, anti-clockwise rotation was defined as positive value and clockwise rotations as negative as shown in Fig. 4. The raw data in Fig. 5 indicates that the tunnel undergoes an ovalization deformation due to the excavation of foundation pit nearby the shield tunnel.

3.2 Data cleaning and association

According to Xie *et al.* (2018), train vibration has a significant impact on the real time monitoring data, and will create outliers. By comparing the raw data during a nonoperational period ("0 to 4h everyday" in Fig. 6) with and raw data during operation ("Fulltime" in Fig. 6), the fluctuation of the measured data during the nonoperational period is much smaller during the operational period.

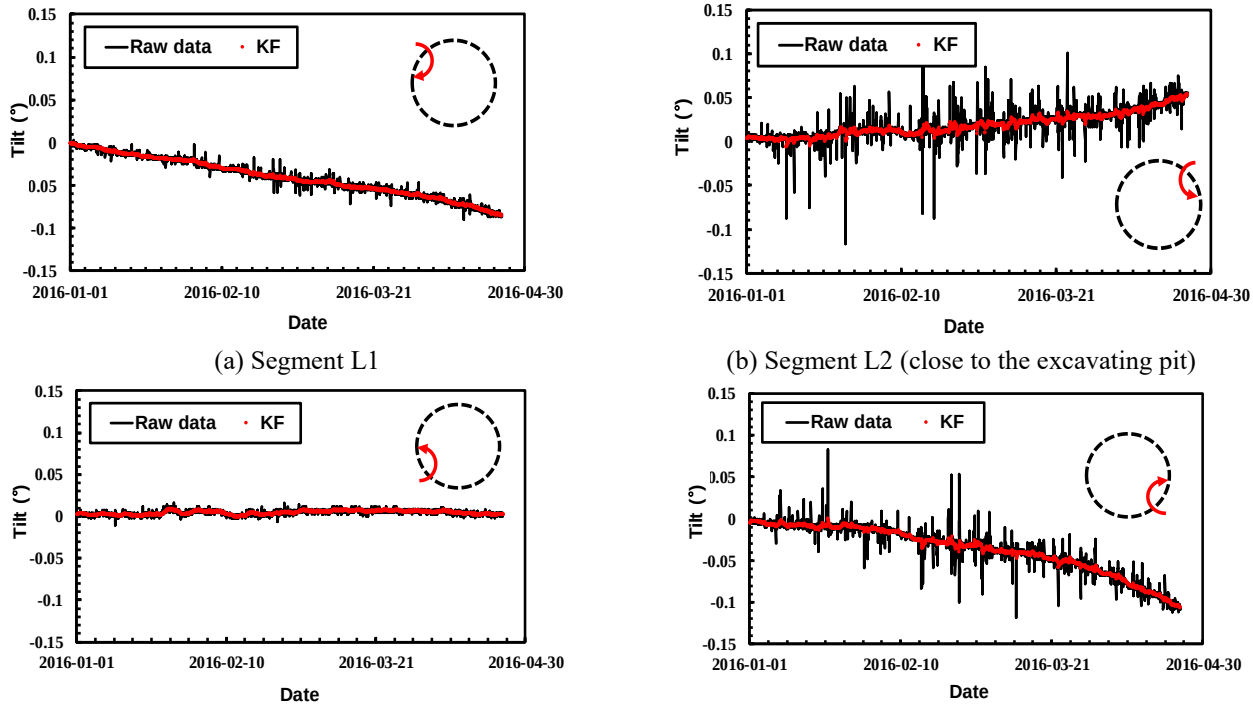

(a) Segment L1 (b) Segment L2 (close to the excavating pit)

(c) Segment B1 (d) Segment B2 (close to the excavating pit)

Fig. 7 Kalman filter (KF) to clean raw data in Fig. 5

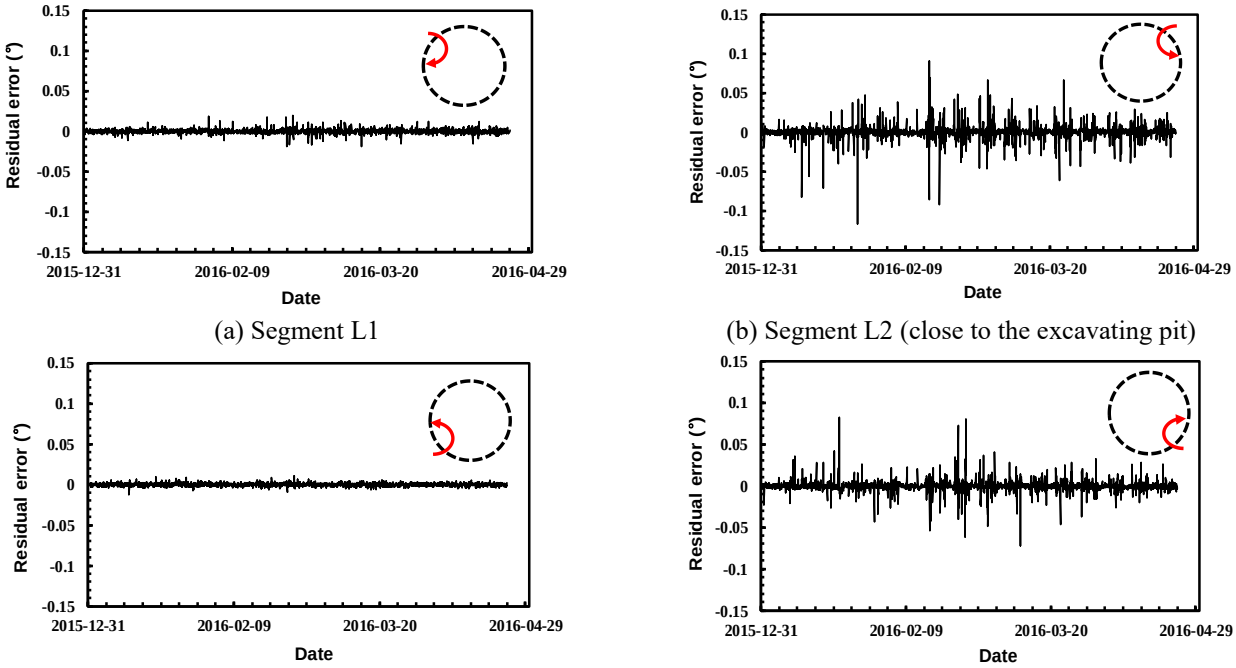

(a) Segment L1 (b) Segment L2 (close to the excavating pit)

(c) Segment B1 (d) Segment B2 (close to the excavating pit)

Fig. 8 Raw data of the tilt sensors at four segments during excavation period

The fluctuation might be attributed to the fact of train vibration. However, this fluctuation is not the interest of this paper as the safety condition of tunnel lining is not dependent on the fluctuation. The Kalman filter was therefore for datacleaning to remove this strong fluctuation.

The real time monitoring data after the Kalman filtering are shown in Fig. 7. It can be seen that the fluctuations are cleaned after the mathematical process and the variation curves of the real time monitoring data are becoming more stable.

Table 1 Coefficients of the response surface function

Coefficient	Y_{L1} (°)	Y_{L2} (°)	Y_{B1} (°)	Y_{B2} (°)	ΔD_h(mm)	ΔD_v(mm)	σ(MPa)	δ(mm)
α_{31}	99.40	-5.31	-6.55	8.60	-679.49	639.33	48000	-50.07
α_{21}	-165.12	10.29	12.93	-15.37	1261.37	-1166.60	-85800	94.18
α_{11}	91.92	-8.23	-10.10	8.82	-845.46	764.05	49900	-65.62
α_{32}	97.84	0.83	-0.10	-0.97	57.49	-36.25	880	3.12
α_{22}	-160.85	-0.75	0.13	0.87	-64.60	48.90 •	-966	-4.09
α_{12}	89.44	-0.70	0.25	1.68	-51.25	35.91	-906	-2.20
α_0	-34.07	2.89	2.64	-2.73	271.36	-236.46	-8230	20.33
R_2	0.982	0.999	0.999	0.999	0.997	0.996	0.932	0.998

Fig. 8 gives the residual error of the Kalman filter. Residual error is defined as the difference between the measured tilt data and the tilt after Kalman filter processing. It is interesting to note that the residual error of segments L2 and B2 shown significantly more fluctuation than segments L1 and B1. The segments close to the excavating foundation pit are therefore more sensitive to the train vibration.

Given that the four tilt sensors in the same section are independent of each other, the time of data collection are not exactly consistent among the four sensors. In this case study, the monitoring system has a high frequency ($20min^{-1}$). Considering that the tunnel is relatively stable within such a short time interval, a linear polynomial interpolation is chosen to keep the data using different sensors consistent with time.

3.3 Numerical simulation

A load-structure model as shown in Fig. 2 was established and analyzed with the Finite Element method (FEM) using the commercial code ABAQUS. The unloading process caused by an adjacent pit excavation is often simulated by decreasing the lateral resistance of the tunnel (Liu *et al.* 2016). Considering that the excavation is on one side of the tunnel, the lateral soil pressure of the two sides are not the same during the excavation. The coefficient of lateral soil pressure K_0 on the distal side and the proximal side were chosen as the external forces x_1 and x_2.

In the numerical model of shield tunnel, the prefabricated segments were modeled with solid elements connected by steel bolts represented by beam elements. There is hard contact between the different segments: a friction coefficient of 0.6 was selected. Therefore, the longitudinal joint opening can be quantified from the displacements of nodes. According to the Chinese code for metro design (GB50157 2013), the coefficient of subgrade reaction is selected based on the empirical judgement or a wide range suggested by code. Therefore, the subgrade reaction of the surroundings is simplified by soil spring. A coefficient of subgrade reaction of 25 MPa/m was selected according to the value in Shanghai district. Both the increment in the lateral earth pressure and the subgrade reaction of the tunnel will increase the deformation and the bending moment of the tunnel lining. However, the analysis will be quite complicated and the data will be overfitted if both lateral earth pressure and subgrade reaction are taken into consideration at the same time. So the subgrade reaction here is assumed to be static for the sake of simplifying the model and improving the calculation efficiency. The coefficient of lateral earth pressure of two sides will be seen as the feature parameters in this case.

The deformation and internal forces on the tunnel change under excavation. In the present case study, the tunnel responses, such as rotation of each of the 4 segments, horizontal and vertical convergence of the tunnel, bolt stresses and joint opening were obtained with different combination of x_1 and x_2. The initial horizontal convergence in this case study is 30 mm which is corresponding to 0.6 for the lateral soil pressure coefficients x_1 and x_2. Fig. 9 shows that segments L1, L2, B1 and B2 rotate due to the nearby excavation. The horizontal and vertical inner diameters of the tunnel have increments of ΔD_h and ΔD_v respectively. Considering that the tunnel has a horizontal convergence, the vertical convergence change ΔD_v is negative when x_1 and x_2 show a decrease. The longitudinal joint opening δ and bolt stress σ should also increase in the construction period.

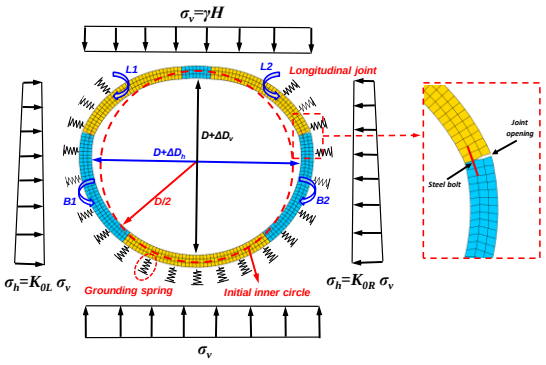

Fig. 9 Tunnel response under the nearby excavation based on the numerical simulation

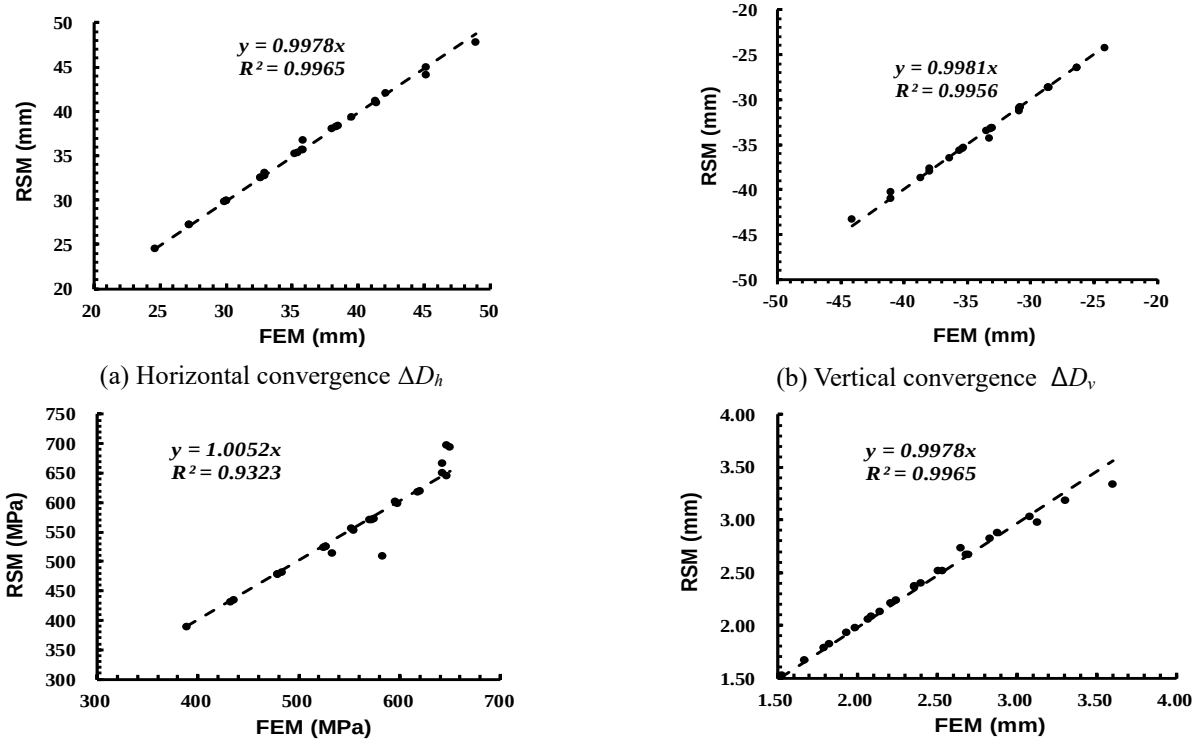

(a) Horizontal convergence ΔD_h (b) Vertical convergence ΔD_v

(c) Bolt stress σ (d) Joint opening δ

Fig. 10 Comparison of displacements, bolt stress and joint opening using response surface method

3.4 Establishing response surface function

The response surface function method is a statistical method to simplify and optimize the relationship between parameters (i.e., find the best set of factors to fit the observed data) (Bucher and Bourgund 1990, Rajashekhar and Ellingwood 1993). A third order polynomial function was established to reflect the relationship between external forces x_1 and x_2 and the tunnel responses

$$\boldsymbol{y} = g(\boldsymbol{x}) + \boldsymbol{\varepsilon} = \sum_{i=1}^{2} \boldsymbol{\alpha}_{3i} x_i^3 + \sum_{i=1}^{2} \boldsymbol{\alpha}_{2i} x_i^2 + \sum_{i=1}^{2} \boldsymbol{\alpha}_{1i} x_i + \boldsymbol{\alpha}_0 + \boldsymbol{\varepsilon} \quad (14)$$

where $\boldsymbol{y}$ is the structure response of the tunnel; g is the response function of $\boldsymbol{y}$; coefficients $\boldsymbol{\alpha}_{3i}$, $\boldsymbol{\alpha}_{2i}$, $\boldsymbol{\alpha}_{1i}$ and $\boldsymbol{\alpha}_0$ are vectors obtained with the least squares method based on the numerical simulations in subsection 3.3; model error $\boldsymbol{\varepsilon}$ expresses the bias between RSM and FEM results.

The range of x_1 and x_2 in the fitting process is from 0.4 to 0.65. This data interval covered whole variation process of the external forces in this case study.

The resulting coefficients of the response surface of the third order are listed in Table. 1. Over 25 points are chosen to check the accuracy of the response surface functions. It should be noted that the order of polynomial function should be chosen based on the practical fitness of the data. As shown in Fig. 10 and Table. 1, the regression coefficient R^2 of the fitting curve is very close to 1. It indicates that the model error ε of RSM is relatively small and it is very effective using the third order polynomial function.

3.5 Extended Kalman filter

The example analysis considers two external forces (x_1 and x_2) and four observation parameters from the four tilt sensors in the same tunnel section. The relationship among the two external forces and four observation parameters can be reflected with the response surface function in Eq. (14)

$$y_m = g_m(\boldsymbol{x}) = \sum_{j=1}^{2} \alpha_{m3j} x_i^3 + \sum_{j=1}^{2} \alpha_{m2j} x_j^2 + \sum_{j=1}^{2} \alpha_{m1j} x_j + \alpha_{m0} \quad (15)$$

where y_1, y_2, y_3, y_4 represent the rotation of segment L1, L2, B1 and B2 respectively, g_m is the response function for the for the observation parameter y_i. The coefficients of gi are those listed in Table 1. The parameter matrix H of the extended Kalman filter (*EKF*) process is a 4×2 matrix

$$H = \frac{\partial \boldsymbol{g}}{\partial \boldsymbol{x}} = \begin{bmatrix} \sum_{i=1}^{3} i\alpha_{1i1} x_1^{(i-1)} & \sum_{i=1}^{3} i\alpha_{1i2} x_2^{(i-1)} \\ \sum_{i=1}^{3} i\alpha_{2i1} x_1^{(i-1)} & \sum_{i=1}^{3} i\alpha_{2i2} x_2^{(i-1)} \\ \sum_{i=1}^{3} i\alpha_{3i1} x_1^{(i-1)} & \sum_{i=1}^{3} i\alpha_{3i2} x_2^{(i-1)} \\ \sum_{i=1}^{3} i\alpha_{4i1} x_1^{(i-1)} & \sum_{i=1}^{3} i\alpha_{4i2} x_2^{(i-1)} \end{bmatrix} \quad (16)$$

The external forces are updated by repeating the process from Eq. (9) to Eq. (13). Monitoring data and an approximate transformation matrix H were used in the updating process.

3.6 Result of data fusion

3.6.1 External forces

Fig. 11 presents the variation in the coefficient of lateral earth pressure during the nearby excavation period. The lateral earth pressure coefficient K_{0R} on the right side (nearest the excavation) dropped from 0.6 to 0.54 in the four-month period. However, the lateral earth pressure coefficient on the left side K_{0L} remained approximately constant over the four-month period. Only a very slight decrease in K_{0L} can be observed. The nearby excavation (Fig. 3) has a significantly larger influence on the closest side of the tunnel.

3.6.2 Tunnel convergence

The tunnel deformations are often used as a key performance indicator (KPI) for the safety and serviceability assessment of a tunnel (Mair 2008, Pinto *et al.* 2014, Liu *et al.* 2016). The ratio of horizontal convergence to initial outer diameter, i.e., $\Delta D/D_{out}$, is one of the most frequently used KPI in codes for tunnel. British Tunnel Standards (BTS, 2004) sets that the ultimate limit of the ratio is about 2%. Given that the outer diameter in most of the Shanghai metro tunnel is 6.2 m, the ultimate limit of the convergence is 124 mm. Figs. 12 and 13 present the horizontal and vertical convergence variation during the monitored nearby excavation period. The horizontal convergence in Fig. 12 and the vertical convergence in Fig 13 indicate that the nearby excavation caused a change of 4mm in both horizontal and vertical convergence. This is still a wide distance to the ultimate limit of 124 mm.

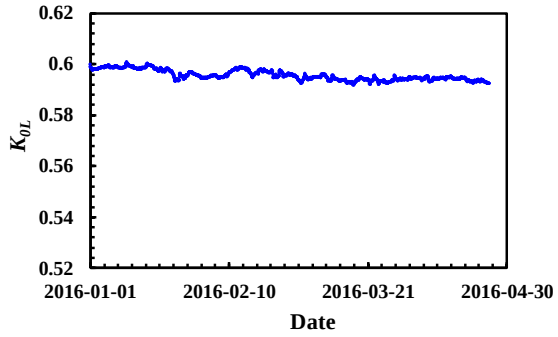

(a) K_0 in the left sides

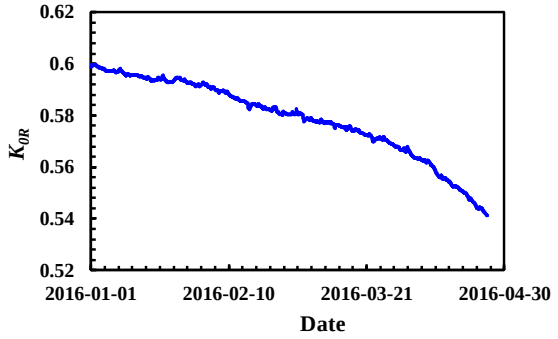

(b) K_0 in the right sides (close to the foundation pit)

Fig. 11 Variation of lateral earth pressure coefficients

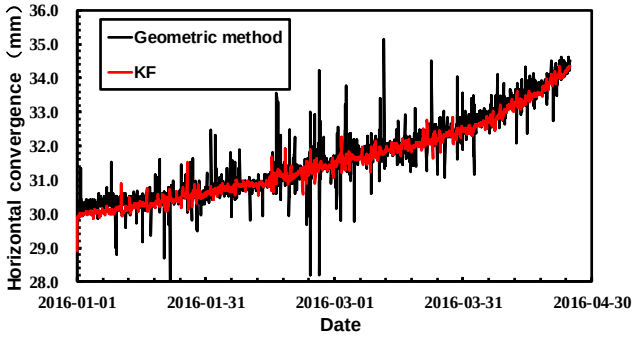

Fig. 12 Horizontal convergence obtained with the data fusion and the geometric method

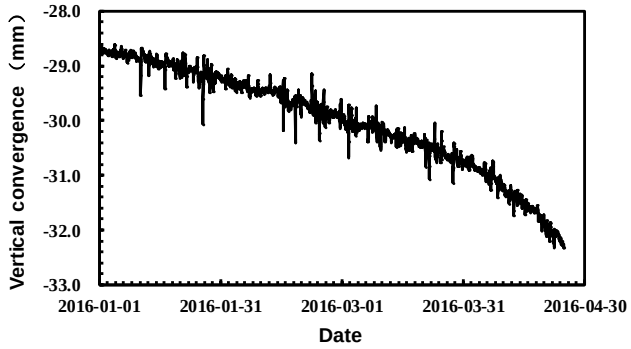

Fig. 13 Vertical convergence obtained with the data fusion method

Zhang (2015) divided the ratio of horizontal convergence into 5 levels: 5‰D_{out}, 8‰D_{out}, 10‰D_{out}, 12‰D_{out}, 14‰D_{out} using statistical analysis of tunnel convergence data in Shanghai Metro Line 2. It can be seen that the horizontal convergence reach the first level (5‰D_{out}) in February in 2016, and it hasn't reach the second level of 8‰D_{out} at the end of the excavation period. The horizontal convergence using the Kalman filter method is similar to the geometric method. The rotation of segment B1 and B2 are used for the geometric method (Figs. 5(c) and 5(d)) Detail information of the geometric method will be introduced in the subsection 3.7.

3.6.3 Segments internal forces and bolt stress in tunnel segments

The axial forces and bending moment in the segment cross sections under different combination of lateral earth pressure were calculated with the FEM model. The relationship among internal forces and external forces were simplified fitted by the response surface functions. The axial forces and bending moments were updated based on the monitoring data in order to evaluate the safety condition of the segment. The bearing capacity was calculated for the ultimate limited state (ULS) ITA (2000). The critical curves for positive and negative moment in the tunnel segments are presented in Fig. 14. None of the internal force combination

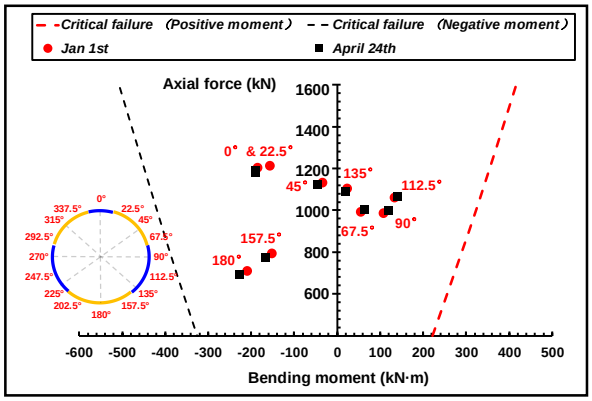

Fig. 14 Spatial distribution of internal forces in different segment sections

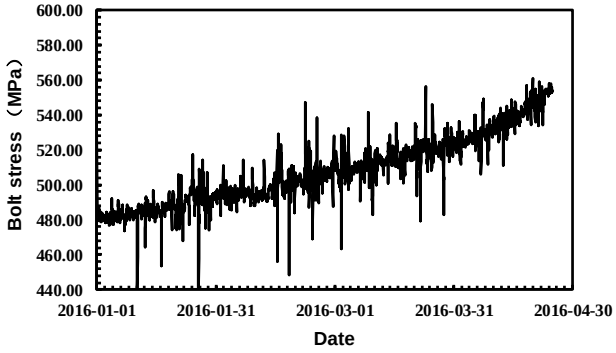

Fig. 15 Bolt stress variation during the period of the nearby excavation

exceed the critical boundaries. Fig. 15 gives the bolt stress at the top longitudinal joint (which is the highest among all other bolts). The bolt stress developed under the excavation nearby reached nearly 560 MPa in April 29th 2019. This stress is well within the safe state as the yield stress is 640MPa.

3.6.4 Opening width and waterproofing of the longitudinal joint

Joints are the weakest part of a tunnel segmental lining. Large joint openings cause not only the bolt fracture but also cause a degradation of waterproofing performance. Hence joint opening width (δ) is often regarded as a key performance index (KPI) for the tunnel safety assessment (Liao *et al.* 2008, Huang *et al.* 2017). The joint opening can also be estimated with the proposed data fusion method. The results are shown on Fig. 16. The joint opening on the right side of the tunnel (close to the excavation) is much larger than on the left side.

Fan *et al.* (2012) pointed out that leakage of the longitudinal joint may occur if the contact stress of the rubber sealer P_0 is not enough to resist the external water pressure P_w

$$P_w > \alpha P_0 \tag{17}$$

where α is usually taken as 0.87.

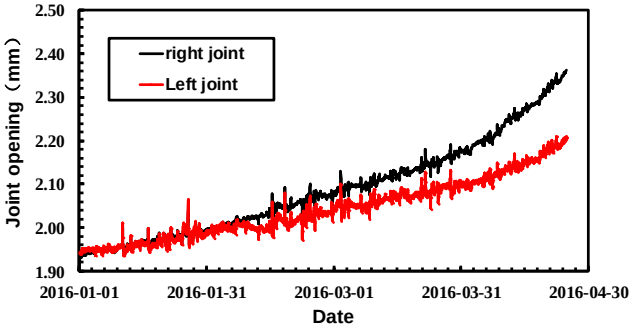

Fig. 16 Variation of joint opening caused by the nearby excavation over four months on left and right side of tunnel

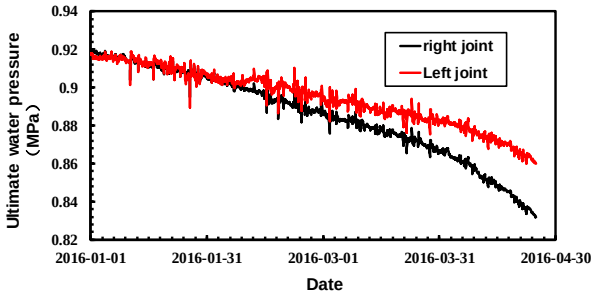

Fig. 17 Ultimate water pressure

The contact stress P_0 can be calculated as

$$P_0 = \frac{rF_s}{A} \tag{18}$$

where r is the residual stress ratio which reflects the working performance of the rubber seal, A is the contact area of the rubber seal and F_s is the extrusion force which can be calibrated with laboratory tests.

The Code for Polymer water-proofing materials (GB18173.4, 2010) specifies that the initial compression displacement is 6 mm. The axial compression displacement Δ can be determined from the longitudinal joint opening δ

$$\Delta = 6 - \delta \tag{19}$$

According to the laboratory test conducted by Yan *et al.* (2011), the extrusion force can be calculated with the following equation

$$F_S = \begin{cases} 0.14\Delta^2 + 2.97\Delta + 0.38 & 0 \le \Delta \le 4mm \\ 7.7\Delta^3 - 105.4\Delta^2 + 488.6\Delta - 746.6 & 4 \le \Delta \le 7mm \end{cases} \tag{20}$$

Using the equation from (17) to (20), the ultimate water pressure can be updated. Fig. 17 shows that the ultimate water pressure of the right joint is higher than that of the left joint as the joint opening of the left joint is much smaller. Given that the depth of the tunnel is 24 m, the hydrostatic pressure is about 0.24MPa. The ultimate water pressure calculated by the proposed method is much more than that of the hydrostatic pressure.

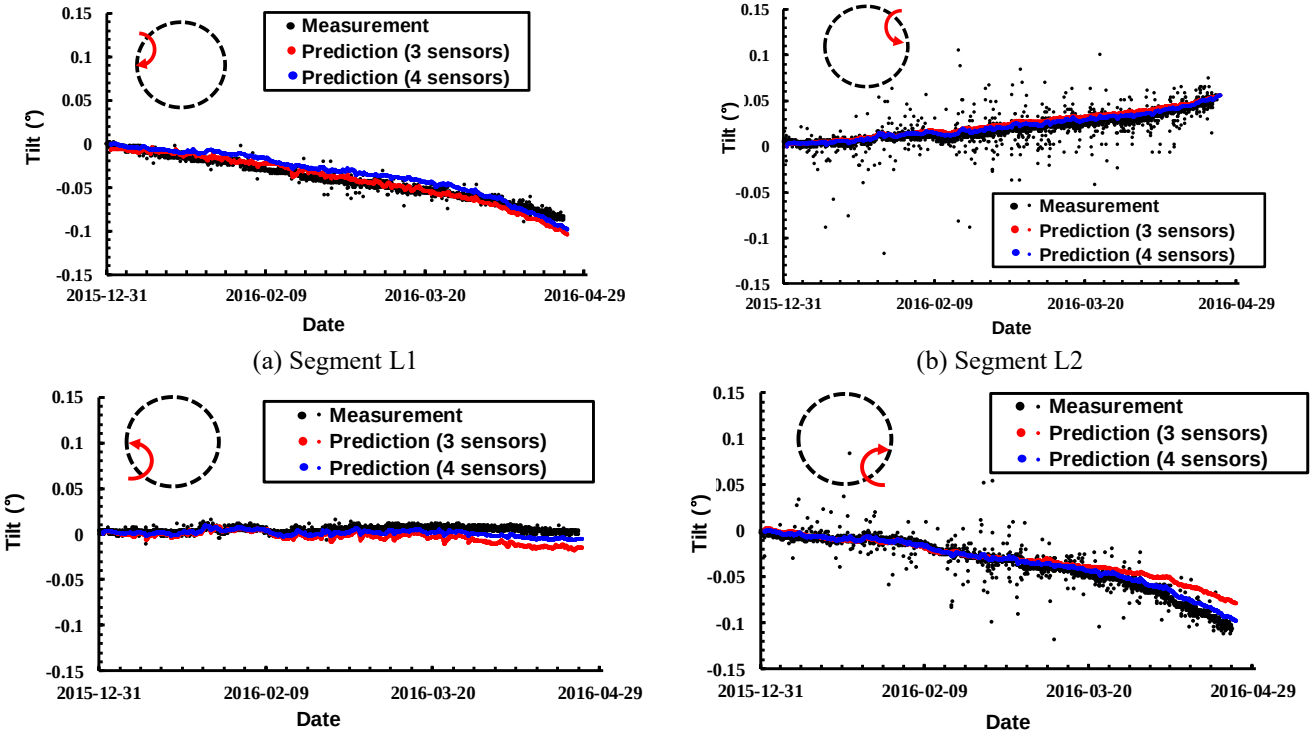

(a) Segment L1 (b) Segment L2

(c) Segment B1 (d) Segment B2

Fig. 18 Comparison of measurement and prediction of tilt

3.7 Verification of the data fusion method

There were four tilt sensors installed in the same cross section (Ring 805) of the tunnel. Each tilt measured by one sensor can be predicted based on the other three sensors with the proposed data fusion method. Fig. 18 compares the measured and predicted tilt, the latter made on the basis of three and four sensors. The predictions in red were done with the data fusion method using the other three tilt data at the same time. The prediction and the actual measurement in segment L1, L2 and B1 match well in Fig. 18. The good match verifies that the rotation of the four segments are not totally independent of each other. The internal correlation of the four rotations were simulated using the load structure model in the proposed method. Considering that the rotation can also be updated using the other three sensors, the data fusion process can improve the robustness of the behavior derived from the monitored data system.

Fig. 18(d) shows that there is a difference of 0.04° (the measurement is 0.11°) between the measurement and prediction values of the rotation of segment B2. However, this difference of 0.04° can be reduced to 0.01° when the data from tilt sensor B2 is taken into use. Given that the sensor in segment B2 measure the rotation directly, some information about the structure response in segment B2 was missing when only the three other sensors were used for the interpretation of the monitoring data. Therefore, the accuracy of the structural response gets improved with more monitoring sensors.

The tunnel convergence quantified using the proposed method was compared with normal geometric method in Fig 12 in order to verify the accuracy of the proposed method. The geometric model frequently used to calculate convergence assumed that segment D is static and segments B rotates around the longitudinal joint between the two segments and the horizontal convergence can be calculated from the tilt data with the geometrical relationship in Fig 19.

$$\Delta D = L\left(\Delta\theta_1 - \Delta\theta_2\right)\cos\omega \tag{21}$$

where ΔD is the change of horizontal convergence; $\Delta\theta_1$ and $\Delta\theta_2$ are the changes of angle which take the anticlockwise as the positive direction; L is the distance from the turning point to the inner surface at the center point level; and ω is the angle between the vertical line and the horizontal diameter of the tunnel (Fig 12).

According to Huang *et al.* (2013) and Wang *et al.* (2016), the geometric method for horizontal convergence calculation had a reasonable high accuracy and is close to the actual convergence change by laser distance meter. Fig. 12 compares the horizontal convergence obtained with the geometric method and with the data fusion method. The horizontal convergence of geometric method is calculated with the rotation of B segments (Figs. 5(c) and 5(d)) using the Eq. (21). The average value of the geometric method and data fusion method are quite similar. The data fusion method is however more stable and has fewer and less spread-out outliers than the geometric model. Hence the data fusion method is reliable for the interpretation of tunnel convergence.

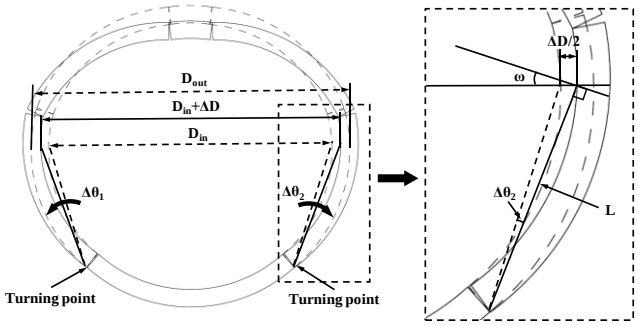

Fig. 19 Geometric model for the horizontal convergence in a shield tunnel

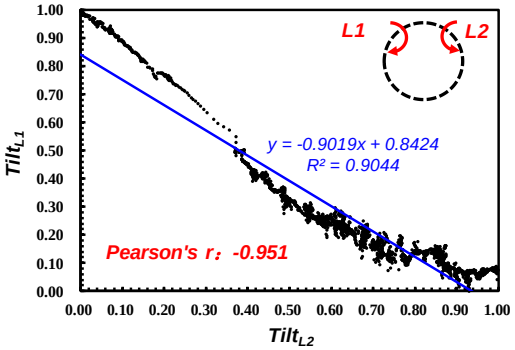

(a) Comparison of $Tilt_{L1}$ and $Tilt_{L2}$

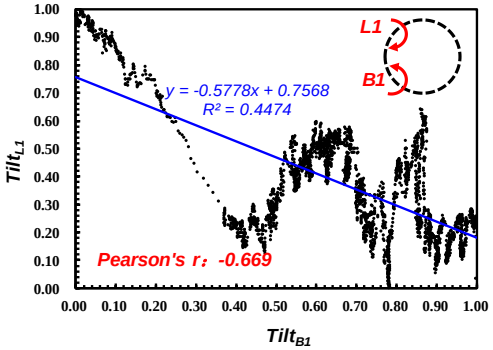

(b) Comparison of $Tilt_{L1}$ and $Tilt_{B1}$

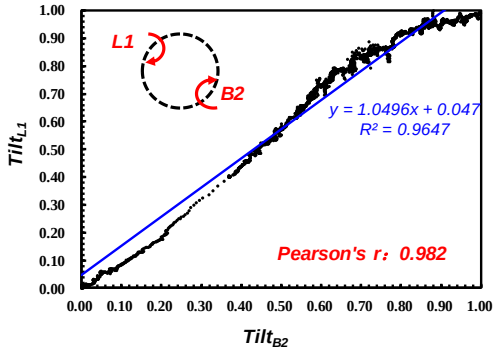

(c) Comparison of $Tilt_{L1}$ and $Tilt_{B2}$

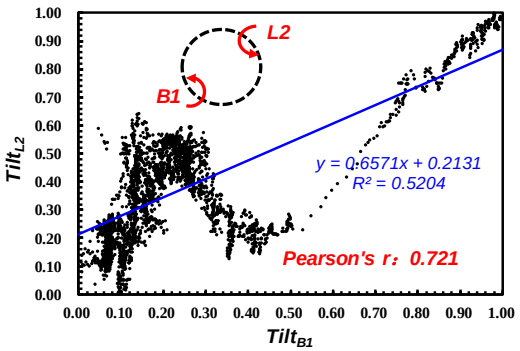

(d) Comparison of $Tilt_{L2}$ and $Tilt_{B1}$

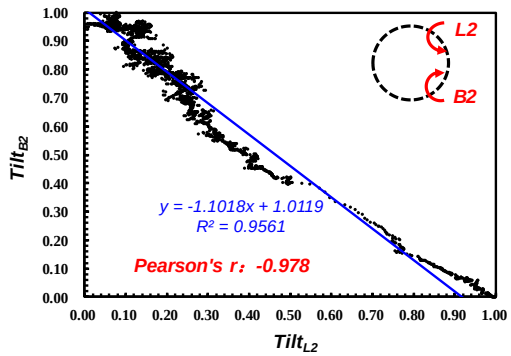

(e) Comparison of $Tilt_{L2}$ and $Tilt_{B2}$

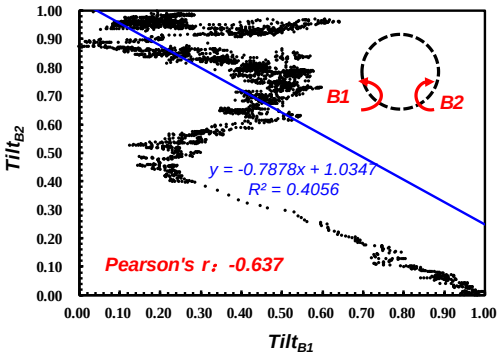

(f) Comparison of $Tilt_{B1}$ and $Tilt_{B2}$

Fig. 20 Comparison of data using different tilt sensors

4. Discussion

4.1 Correlation among monitoring data

In practice, the monitoring data using different sensors may be correlated with each other. However, it is difficult to express the correlation directly based on the usual mechanical analysis. Hence, novel inverse analysis approaches have been proposed to make a holistic assessment of the data (Peng *et al.* 2014).

Fig. 20 shows the comparison of tilt data from different sensors. The data were normalized before data cleaning by Kalman filter (Fig 7). Tilt data of segment L1 has a strong negative correlation with that of segment L2 and B2. The Pearson correlation coefficients are closing to -1. In addition, there is a positive correlation between the tilt data of segment L1 and B2. The correlation is quite strong as the Pearson correlation coefficient is closing to 1. The tilt of segment B1 has relatively weak correlation with the data from other three tilt sensors. It can be seen from Figure 7 that nearby construction has little effect on the rotation of segment B1. Nevertheless, the Pearson correlation coefficient is larger than 0.5 or smaller than -0.5. Thus, it can be seen that the data using different sensors are correlated with each other in the construction period.

More importantly, the proposed data fusion approach provides us a global interpretation to understand the tunnel response under external stress changes. The nearby construction or other event can lead to a disturbance of the soil which may change the structure response of the tunnel, and variation in the monitoring data. The relationship between structure response and the external forces were established based on a simplified numerical model. Fig. 18 shows that the change in rotation variations of the four segments in the same cross section (Ring 805) are not totally axisymmetric especially segment B1 and B2. According to the numerical result in Fig. 11, the coefficient of lateral earth pressure on the two sides of the tunnel are different in space. The disturbance due to the nearby excavation on the soil on the right side is larger than that on the left side. Given that the tunnel is a long continuous structure similar to a long strip, this leads to a constrained condition in the surrounding soil especially the soil on the left side, opposite to the excavating pit.

4.2 Limitation of the proposed method

The proposed data fusion approach has limitations that should be improved in the future:

(1) The failure of a shield tunnel may involve several characteristics such as large convergence change, fracture of bolts, concrete spalling and waterproof failure. How to identify the likely failure mechanisms of the shield tunnel and how to define the ultimate state of the system are subject of further research, and is at present not easily modelled with the data fusion approach.

(2) The time effect of monitoring information should be considered in the future, especially long term effects, which may be caused by aging bolts, concrete crack development, soil creep, tunnel leakage and so on.

(3) The method uncertainty (bias and variability) of the numerical simulation should be considered in practical applications. The accuracy of the data fusion approach depends on the result of the numerical model. The influence of the method uncertainty on the data fusion result should be studied in order to improve the reliability of the safety assessment.

5. Conclusions

This paper presented a novel method for tunnel safety evaluation utilizing multi-sensor monitoring data. The following conclusions can be drawn:

(1) A data fusion framework is constructed by integrating several real time monitoring sensors. The interrelationships among the external loads, monitoring information, tunnel responses and performances are included in the proposed analysis framework. Tunnel performance indexes such as maximum factor of safety and ultimate water pressure were quantified with finite element analysis and response surface fitting function.

(2) Different sources of monitoring information in the same cross-section of a tunnel can be taken into account in the safety evaluation with the proposed multi-sensor data fusion method. The extended Kalman filter method was used to integrate the different monitoring data and estimate the impact of nearby construction through the updating of the external forces affecting the tunnel performance. The updated result showed that the coefficient of lateral earth pressure became asymmetrical due to a nearby excavation.

(3) Different monitoring data in the same cross-section were correlated with each other during the nearby excavation of a foundation pit. The monitoring data from one sensor can be estimated using the monitoring data from the other sensors in the same cross section. The comparison of the measurement and prediction indicate that the accuracy will be improved with additional sensors.

(4) The correlations among different monitoring data and the method uncertainty of the finite element method should be studied in the future to make the safety evaluation approach more robust and more reliable.

Acknowledgments

This study is substantially supported by the Natural Science Foundation Committee Program (No. 51538009, 51608380), by Shanghai Rising-Star Program (17QC1400300) and by Key innovation team program of innovation talents promotion plan by MOST of China (No. 2016RA4059). Hereby, the authors are grateful to these programs. And the authors are grateful to the Research Council of Norwegian Geotechnical Institute.

References

Bennett, P. J., Soga, K., Wassell, I., Fidler, P., Abe, K., Kobayashi, Y. and Vanicek, M. (2010a), "Wireless sensor networks for underground railway applications: Case studies in Prague and

London", *Smart Struct. Syst*., **6**(5-6), 619-639. https://doi.org/10.12989/sss.2010.6.5_6.619.

Bennett, P.J., Kobayashi, Y., Soga, K. and Wright, P. (2010b), "Wireless sensor network for monitoring transport tunnels", *Proc. Inst. Civ. Eng. Geotech. Eng.*, **163**, 147-156. DOI: 10.1680/geng.2010.163.3.147.

Bhalla, S., Yang. Y.W., Zhao. J. and Soh, C.K. (2005), "Structural health monitoring of underground facilities – Technological issues and challenges", *Tunn. Undergr. Sp. Tech.*, **20**, 487-500. DOI: 10.1016/j.tust.2005.03.003.

BTS (2004), Tunnel lining design guide, British Tunneling Society Institution of Civil Engineers, London: Thomas Telford.

Bucher, C.G. and Bourgund, U. (1990), "A fast and efficient response surface approach for structural reliability problems", *Struct. Saf.*, **7**, 57-66. DOI:10.1016/0167-4730(90)90012-E.

Bucher, C. G. and Most, T. (2008), "A comparison of approximate response functions in structural reliability analysis", *Probabilist. Eng. Eng. Mech.*, **23**, 154-163. DOI: 10.1016/j.probengmech.2007.12.022.

Chen, J.J., Zhang, W. and Wang, J.H. (2017), "Data Fusion Analysis Method for Assessment on Safety Monitoring Results of Deep Excavations", *J. Aerosp. Eng*., **30**, B4015005. DOI: 10.1061/(ASCE)AS.1943-5525.0000593.

Doležalov, M. (2001), "Tunnel complex unloaded by a deep excavation", *Comput. Geotech.*, **28**, 469-493. DOI: 10.1016/s0266-352x(01)00005-2.

Erazo, K. and Hernandez, E.M. (2016), "Bayesian model–data fusion for mechanistic postearthquake damage assessment of building structures", *J. Eng. Mech.*., **142**, 04016062. DOI: 10.1061/(ASCE)EM.1943-7889.0001114.

Fan, Q.G., Fang, W.M. and Su, X.B. (2002), "Experimental study on the waterproof capability of the hydro-expansive rubber sealing cushion in shield tunnel", *Underg. Space*., **22**, 335-338. (in Chinese)

Frangopol, D.M. (2008), "Probability concepts in engineering: emphasis on applications to civil and environmental engineering", *Struct. Infrastruct. Eng.*, **4**, 413-414. DOI: 10.1080/15732470802027894.

GB18173.4 (2010), Code for Polymer Water-proof Materials-Part 4: Rubber Gasket for Shield-Driven Tunnel, Beijing, China (in Chinese).

GB50157 (2013), Code for design of metro. Beijing: Ministry of Housing and Urban-rural Development of China, Beijing, China (in Chinese).

Hall, D. L. and Llinas, J. (1998), "An introduction to multi-sensor data fusion", *Int. Symp. Circuits Sys.*, 6-23. DOI: 10.1109/ISCAS.1998.705329.

Housner, G.W., Bergman, L.A., Caughey, T.K., Chassiakos, A.G., Claus, R.O., Masri, S.F., Skelton, R.E., Soong, T.T., Spencer. B. F. and Yao, J.T.P. (1997), "Structural control: past, present, and future", *J. Eng. Mech*., **123**, 897-971. DOI: 10.1061/(ASCE)0733-9399(1997)123:9(897).

Hu, X., Wang, B. and Ji, H. (2013), "A wireless sensor network-based structural health monitoring system for highway bridges", *Comput. Aided Civil Infrastruct. Eng.*, **28**, 193-209. DOI: 10.1111/j.1467-8667.2012.00781.x.

Huang, H.W., Shao, H., Zhang, D.M. and Wang, F. (2017), "Deformational responses of operated shield tunnel to extreme surcharge: a case study", *Struct. Infrastruct. Eng.*, **13**, 345-360. DOI: 10.1080/15732479.2016.1170156.

Huang, H.W., Xu, R. and Zhang, W. (2013), "Comparative performance test of an inclinometer wireless smart sensor prototype for subway tunnel", *Int. J. Architect. Eng. Constr.*, **2**, 25-34.

International Tunneling Association (ITA). (2000), "Guidelines for the design of shield of tunnel lining", *Tunn. Undergr. Sp. Tech.*, **15**(3), 303-331. DOI: 10.1016/s0886-7798(00)00058-4.

Kalman, R.E. (1960), "A new approach to linear filtering and prediction problems", *J. Basic Eng. Trans*., **82**, 35-45. DOI:10.1115/1.3662552.

Liu, J.F., Wang, H.F, Ge, Y. and Huang, J.L. (2013), "Application of multi-source information fusion technology in the construction of a secure and emergent transportation platform", *ICTIS 2013*, 237-243.

Li, X.Y., Zhang, L.M. and Jiang, S.H. (2016a), "Updating performance of high rock slopes by combining incremental time-series monitoring data and three-dimensional numerical analysis", *Int. J. Rock Mech. Min. Sci*., **83**, 252-261. DOI: 10.1016/j.ijrmms.2014.09.011.

Li, X.Y., Zhang, L.M., Jiang, S.H., Li, D.Q. and Zhou, C.B. (2016b), "Assessment of slope stability in the monitoring parameter space", *J. Geotech. Geoenviron. Eng.*, **142**, 04016029. DOI: 10.1061/(ASCE)GT.1943-5606.0001490.

Liao, S.M., Peng, F.L. and Shen, S.L. (2008), "Analysis of shearing effect on tunnel induced by load transfer along longitudinal direction", *Tunn. Undergr. Sp. Tech.*, **23**, 421-430. DOI: 10.1016/j.tust.2007.07.001.

Liu, X., Bai, Y., Yuan, Y. and Mang, H.A. (2016), "Experimental investigation of the ultimate bearing capacity of continuously jointed segmental tunnel linings", *Struct. Infrastruct. Eng.*, **12**, 1-16. DOI: 10.1080/15732479.2015.1117115.

Mair, R.J. (2008), "Tunnelling and geotechnics: new horizons", *Geotech.*, 58, 695-736. DOI: 10.1680/geot.2008.58.9.695.

Mohamad, H., Soga, K., Bennett, P.J., Mair, R. J. and Lim, C.S. (2012), "Monitoring twin tunnel interaction using distributed optical fiber strain measurements", *J. Geotech. Geoenviron. Eng.*, **138**, 957-967. DOI: 10.1061/(ASCE)GT.1943-5606.0000656.

Ou, J.P. (2003), "Some recent advances of structural health monitoring systems for civil infrastructure in mainland China", *P. Int. Conf. Struct. Health Moni. Intell. Infrastruct.*, Tokyo, Japan, 131-144. DOI: 10.1117/12.634044.

Peng, M., Li, X.Y., Li, D.Q., Jiang, S.H. and Zhang, L.M. (2014), "Slope safety evaluation by integrating multi-source monitoring information", *Struct. Saf*., **49**, 65-74. DOI: 10.1016/j.strusafe.2013.08.007.

Pinto, F. and Whittle, A.J. (2014), "Ground movements due to shallow tunnels in soft ground. I: analytical solutions", *J. Geotech. Geoenviron. Eng.*, **140**, 04013040. DOI: 10.1061/(ASCE)GT.1943-5606.0000948.

Rajashekhar, M.R. and Ellingwood, B.R. (1993), "A new look at the response surface approach for reliability analysis", *Struct. Saf*., **12**, 205-220. DOI:10.1016/0167-4730(93)90003-J.

Santos, F.L., Jesus, V.A.M.D. and Valente, D.S.M. (2012), "Modeling of soil penetration resistance using statistical analyses and artificial neural networks", *Acta Sci.-Agron.*, **34**, 219-224. DOI:10.4025/actasciagron.v34i2.11627.

Sharma, J.S., Hefny, A.M., Zhao, J. and Chan, C.W. (2001), "Effect of large excavation on deformation of adjacent MRT tunnels", *Tunn. Undergr. Space Technol. Incor. Trenchless Tech. Res*., **16**, 93-98. DOI: 10.1016/S0886-7798(01)00033-5.

Sun, J., Zhang, J. and Wang, X. (2012), "Multi-sensor data fusion and target location in pipeline monitoring and a pre-warning system based on multi-seismic sensors", *ICPTT.*, Wuhan, China, 961-974. DOI: 10.1061/9780784412619.099.

Torbol, M., Gomez, H. and Feng, M. (2013), "Fragility analysis of highway bridges based on long-term monitoring data", *Comput. Aided Civil Infrastruct. Eng.*, **28**, 178-192. DOI: 10.1111/j.1467-8667.2012.00805.x.

Waltz, E. and Llinas, J. (1990), *Multi. data fus.*, Artech house, Boston, USA.

Wang, F., Huang, H.W., He, B., Wu. Y., Shao. H. and Wu. H.M. (2016), "Wireless sensing on shield tunnels in Shanghai"; *P. Int. Conf. Smart Infrastruct. Cons.*, Cambridge, United Kingdom,

June.

Wang, F., Ling, X., Xun, X. and Feng, Z. (2014), "Structural stiffness identification based on the extended kalman filter research", *Abs. Appl. Ana.*, 1-8. DOI: 10.1155/2014/103102.

Welch, G. and Bishop, G. (2001), "An introduction to the kalman filter", University of North Carolina at Chapel Hill. DOI: 10.1145/800233.807054.

Xie, X., Zhang, D. and Huang, H. (2018), "Data analysis of shield tunnel deformation from real-time monitoring with wireless sensing network", *P. Int. Conf. Tunn. Undergr. Space Technol.*, Shanghai, China, May. DOI: 10.1007/978-981-13-0017-2_40.

Yang, Y., Xu, J. and Soh, C.K. (2005), "Generic impedance-based model for structure-piezoceramic interacting system", *J. Aerospace Eng.*, **18**, 93-101. DOI: 10.1061/(asce)0893-1321(2005)18:2(93).

Ye, X.W., Ni, Y.Q., Wai, T.T., Wong, K.Y., Zhang, X.M. and Xu, F. (2013), "A vision-based system for dynamic displacement measurement of long-span bridges: algorithm and verification", *Smart Struct. Syst*, **12**(3-4), 363-379. https://doi.org/10.12989/sss.2013.12.3_4.363.

Ye, X.W., Yi, T.H., Wen, C. and Su, Y.H. (2015), "Reliability-based assessment of steel bridge deck using a mesh-insensitive structural stress method", *Smart. Struct. Syst.*, **16**(2), 367-382. https://doi.org/10.12989/sss.2015.16.2.367.

Ye, X.W., Dong, C.Z. and Liu, T. (2016), "Image-based structural dynamic displacement measurement using different multi-object tracking algorithms", *Smart Struct. Syst.*, **17**(6), 935-956. https://doi.org/10.12989/sss.2016.17.6.935.

Zhang, D. M., (2015), "Performance-based design and its resilience analysis of underground structure in multi-layered ground", Ph.D. Dissertation, Tongji University, Shanghai. (in Chinese).